Design of implantable MEMS sensors for early stenosis detection

Y. L. Young[1], C. A. Steeves[2], Z. Liu[1] & W. O. Soboyejo[2]
[1] *Department of Civil and Environmental Engineering, Princeton University, Princeton, U. S. A.*
[2] *Department of Mechanical and Aerospace Engineering, Princeton University, Princeton, U. S. A.*

Abstract

This paper examines the design of implantable micro-electro-mechanical systems (MEMS) for long-term *in situ* monitoring of blood flow. The objective is to develop a smart wireless sensing unit for early stenosis detection. The design includes considerations of non-Newtonian hemodynamics, nonlinear material behavior of the vessel wall and fatty plaque buildup, sensitivity and reliability of the sensors, as well as the use of surface coatings for biocompatibility and non-adhesion of blood constituents. Overviews of the fluid model, material model, sensor design configuration, and surface coating selection are presented. Finally, implications of the results are discussed.
Keywords: biomechanics, hemodynamics, MEMS sensors, *in situ* monitoring.

1 Introduction

Stenosis is the narrowing, stiffening, thickening, fusion, or blockage of blood vessels. It is usually caused by plaque buildup, and it can be an extremely serious problem, particularly when it occurs in the blood vessels around the heart. Common corrective procedures include bypass surgery, balloon angioplasty, and stenting. Unfortunately, restenosis often occurs after corrective surgery [1, 2]. Thus, methods to continuously monitor potential stenosis growth and to assess the degree of stenosis are needed. Currently, the "golden standard" for stenosis diagnosis is x-ray angiography(CA) [3, 4], which is an invasive and potentially hazardous procedure. Non-invasive imaging techniques, such as computer tomography angiography(CT), magnetic resonance angiography (MRA), and duplex ultrasound, are also

available. However, most of the non-invasive techniques are operator dependent and/or expensive. In addition, none of the methods are appropriate for extended or continuous monitoring. Thus, the motivation of this work is to develop wireless MEMS sensors for continuous, non-invasive, *in situ* monitoring of blood flow. As suggested in [5], these sensors can be easily implanted during bypass surgery or stenting procedures. The current objectives are to systematically address the selection of hemodynamic parameter for early stenosis detection, the effect of potential fatty plaque buildup and vessel wall characteristics on sensor measurements, the required material behavior to ensure adequate strength and durability, and the necessary properties of the surface coating to guarantee biocompatibility and to resist potential adhesion of blood constituents.

2 Hemodynamic parameter selection

Since the MEMS sensors need to be implanted during bypass or stenting surgeries, the number of sensors should be limited to a minimum. In addition, to justify the effort and cost of implanting the sensor units, the sensors should be able to detect flow abnormality at an early stage and provide a quantitative estimate of the degree of the stenosis. Thus, it is critical to determine the optimal hemodynamic parameter for early stenosis detection.

Traditionally, the peak total pressure drop across the stenotic region has been used as the primary hemodynamic indicator for stenosis assessment. However, as demonstrated in the study presented in [6], the change in peak total pressure drop is only approximately 25% for 60% stenosis. Recently, the internal pressure-flow loop area (PFLA) was proposed by [7, 8] as an alternative parameter for stenosis assessment. Results from their *in vitro* studies shown that the PFLA increased significantly with increasing degree of stenosis, but results from their *in vivo* studies shown that the PFLA did not vary significantly, and even decreased, with increasing stenosis (see data in Table 4 in [8]). Thus, one of the objectives of this work is to explore and compare possible hemodynamic parameters for stenosis assessment via systematic computational fluid dynamics (CFD) simulations. The hemodynamic indicators to be compared include: peak pressure drop; peak wall shear stress; peak velocity; and rate of energy dissipation. The most difficult parameter to measure experimentally is the peak wall shear stress due to the need to obtain the velocity and velocity gradient very near the wall in pulsatile flow. However, the wall shear stress is an important parameter because it has been shown to affect the response and properties of the vessel walls [9] and correlate with sites of atherosclerotic lesions and stenotic regions [10].

2.1 Fluid model

To systematically compare the hemodynamic parameters, a CFD solver is developed to investigate the flow characteristics, and to identify the parameter that best correlates with the degree of stenosis. Following the work in Ref. [11] and many others, the modeled stenotic vessel is assumed to be axisymmetric, and the vessel

radius $R(x)$ is described by the following cosine curve:

$$R(x) = 1 - \frac{a}{2}[1 + cos(\frac{\pi x}{x_0})]; \quad (-x_0 \leq x \leq x_0)$$

$$R(x) = 1; \quad (|x| \geq x_0). \tag{1}$$

A graphical depiction of the model geometry and an example of the numerical grid is shown in Fig. 1. The non-dimensional stenosis length and height are denoted by $2x_0$ and a, respectively.

In the fluid model, the blood is assumed to be an isotropic, homogeneous, and non-Newtonian. The vessel wall is assumed to be rigid, and the flow is assumed to be incompressible, laminar, and axisymmetric. Due to lack of a suitable viscoelastic model for the whole blood, the generalized Newtonian model is adopted for the current flow simulation. The model ignores the effect of blood elasticity, but accounts for the effect of shear thinning (the dominant non-Newtonian effect of whole blood). The Herschel-Bulkley(HB) model is used to relate the dynamic viscosity (μ) with the instantaneous shear rate ($\dot{\gamma}$) because it can capture the shear-thinning property of blood for a wide range of shear rates [12]:

$$\mu(\dot{\gamma}) = \frac{\tau_y}{\dot{\gamma}} + \mu_0 \dot{\gamma}^{n-1}; \quad (\dot{\gamma} \geq \dot{\gamma}_c)$$

$$\mu(\dot{\gamma}) = \frac{\tau_y(2 - \dot{\gamma}/\dot{\gamma}_c)}{\dot{\gamma}_c} + \mu_0[(2 - n) + (n - 1)\frac{\dot{\gamma}}{\dot{\gamma}_c}]\dot{\gamma}_c^{n-1}; \quad (\dot{\gamma} < \dot{\gamma}_c) \tag{2}$$

where τ_y is the yield stress, n is the power index, $\dot{\gamma}_c$ is the critical shear rate, and μ_0 is the consistent viscosity (i.e. the Newtonian dynamic viscosity).

The nondimensionalized governing equation can be rewritten in the form of the streamfunction-vorticity equations in cylindrical coordinates:

$$\frac{\partial \omega}{\partial t} + \frac{1}{r}\frac{\partial \psi}{\partial r}\frac{\partial \omega}{\partial x} - \frac{1}{r}\frac{\partial \psi}{\partial x}\frac{\partial \omega}{\partial r} + \frac{\omega}{r^2}\frac{\partial \psi}{\partial x}$$

$$= \frac{1}{Re}[(\frac{\partial^2 \omega}{\partial x^2} + \frac{\partial^2 \omega}{\partial r^2} + \frac{1}{r}\frac{\partial \omega}{\partial r} - \frac{\omega}{r^2})\zeta + 2\frac{\partial \zeta}{\partial x}\frac{\partial \omega}{\partial x} + \frac{\partial \zeta}{\partial r}(2\frac{\partial \omega}{\partial r} + \frac{\omega}{r})$$

$$+2\frac{\partial^2 \zeta}{\partial xr}(\frac{1}{r^2}\frac{\partial \psi}{\partial x} - \frac{2}{r}\frac{\partial^2 \psi}{\partial xr}) + (\frac{\partial^2 \zeta}{\partial x^2} - \frac{\partial^2 \zeta}{\partial r^2})(\frac{1}{r}\frac{\partial^2 \psi}{\partial r^2} - \frac{1}{r}\frac{\partial^2 \psi}{\partial x^2} - \frac{1}{r^2}\frac{\partial \psi}{\partial r})] \tag{3}$$

$$-\omega r = \frac{\partial^2 \psi}{\partial x^2} + \frac{\partial^2 \psi}{\partial r^2} - \frac{1}{r}\frac{\partial \psi}{\partial r} \tag{4}$$

where ψ and ω are the scalar streamfunction and vorticity, respectively, and are defined as follows:

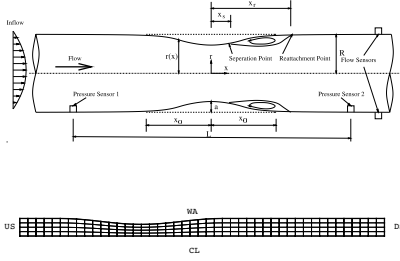$$\omega \equiv \frac{\partial v}{\partial x} - \frac{\partial u}{\partial r} \tag{5}$$

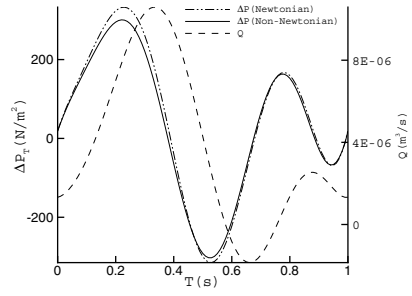Figure 1: Modeled stenotic vessel and corresponding numerical mesh.

Figure 2: Phase lag between ΔP_T and Q for physiological flow.

$$u \equiv \frac{1}{r}\frac{\partial \psi}{\partial r}; \quad v \equiv -\frac{1}{r}\frac{\partial \psi}{\partial x} \tag{6}$$

$\zeta \equiv \frac{\mu(\dot{\gamma})}{\mu_0}$ is the nondimensional dynamic viscosity. The required shear rate for the HB model (Eqn. (2)) is obtained as follows:

$$\dot{\gamma}^2 = \frac{4}{r^2}\left[\frac{1}{r^2}\left(\frac{\partial \psi}{\partial x}\right)^2 + \left(\frac{\partial^2 \psi}{\partial xr}\right)^2 - \frac{1}{r}\frac{\partial \psi}{\partial x}\frac{\partial \psi^2}{\partial xr}\right] + \frac{1}{r^2}\left(\frac{\partial^2 \psi}{\partial r^2} - \frac{1}{r}\frac{\partial \psi}{\partial r} - \frac{\partial^2 \psi}{\partial x^2}\right)^2 \tag{7}$$

The total pressure, $P = p + \frac{1}{2}(u^2 + v^2)$, can be computed as:

$$
\begin{aligned}
\frac{\partial P}{\partial x} &= -\frac{\partial u}{\partial t} + v\omega + \frac{1}{Re}\left[\zeta\left(-\frac{\partial \omega}{\partial r} - \frac{\omega}{r}\right) + \frac{2}{r}\frac{\partial \zeta}{\partial x}\frac{\partial^2 \psi}{\partial xr}\right. \\
&\quad \left. + \frac{\partial \zeta}{\partial r}\left(\frac{1}{r}\frac{\partial^2 \psi}{\partial r^2} - \frac{1}{r}\frac{\partial^2 \psi}{\partial x^2} - \frac{1}{r^2}\frac{\partial \psi}{\partial r}\right)\right] \\
\frac{\partial P}{\partial r} &= -\frac{\partial v}{\partial t} - u\omega + \frac{1}{Re}\left[\zeta\frac{\partial \omega}{\partial x} + \frac{\partial \zeta}{\partial x}\left(\frac{1}{r}\frac{\partial^2 \psi}{\partial r^2} - \frac{1}{r}\frac{\partial^2 \psi}{\partial x^2} - \frac{1}{r^2}\frac{\partial \psi}{\partial r}\right)\right. \\
&\quad \left. + \frac{\partial \zeta}{\partial r}\left(\frac{2}{r^2}\frac{\partial \psi}{\partial x} - \frac{2}{r}\frac{\partial^2 \psi}{\partial xr}\right)\right]
\end{aligned}
\tag{8}
$$

The shear stress at the wall, T_{ns}, can be computed from the Cauchy's stress equation of motion, which can be expressed as:

$$T_{ns} = \zeta\left[2\left(n_x s_x \frac{\partial u}{\partial x} + n_r s_r \frac{\partial v}{\partial r}\right) + (n_x s_r + n_r s_x)\left(\frac{\partial u}{\partial r} + \frac{\partial v}{\partial x}\right)\right] \tag{9}$$

where $\mathbf{n} = [n_r, n_\theta, n_x]$ and $\mathbf{s} = [s_r, s_\theta, s_x]^T$ are the unit normal and tangent vectors, respectively, at the wall.
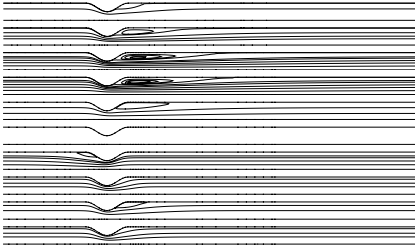
Figure 3: Predicted streamlines for physiological Newtonian flow.
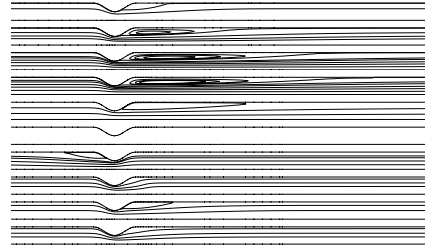
Figure 4: Predicted streamlines for physiological non-Newtonian flow.

At the upstream (Ω_{US}) and downstream (Ω_{DS}) boundaries, the traction free boundary condition is applied:

$$\frac{\partial \psi^2}{\partial xr} = 0 \quad \text{and} \quad \frac{\partial \psi}{\partial x} = 0 \quad \text{at } \Omega_{US} \text{ \& } \Omega_{DS} \tag{10}$$

The vorticity is obtained using Eqn. (3), and the inflow velocities are calculated using Eqn. (6).

At the centerline (Ω_{CL}), the axisymmetric boundary condition is applied. The streamfunction at the centerline is taken to be zero for convenience, and the axial velocity can be calculated using L'Hospital's rule:

$$\psi = 0; \quad \omega = 0; \quad \frac{\partial \mu}{\partial r} = 0; \quad v = 0; \quad u = \lim_{r \to 0} \frac{1}{r}\frac{\partial \psi}{\partial r} = \frac{\partial^2 \psi}{\partial r^2} \quad \text{at } \Omega_{CL} \tag{11}$$

At the vessel wall (Ω_{WA}), the no-slip and no-penetration boundary conditions are applied, and the streamfunction is related to the local flow rate Q:

$$u = 0; \quad v = 0; \quad \psi = \frac{Q}{2\pi U_0 R^2} \quad \text{at } \Omega_{WA} \tag{12}$$

The wall vorticity is calculated by applying Eqn.(3) using a second-order central difference scheme.

In the current formulation, the primary variables to be solved at each time step are ψ and ω, which are governed by Eqns. (3) and (4). A third-order low-storage Runge-Kutta scheme [13] is applied for the time integration of Eqn. (3), and a point-successive-over-relaxation ($PSOR$) method [14] is applied to solve Eqn. (4). The instantaneous shear rate is computed using Eqn.(7). The velocity, pressure, and wall shear stress are obtained from the post-processing of the primary variables using Eqns. (6), (8), and (9), respectively. The solution is obtained iteratively until the periodic condition is satisfied for pulsatile flows, or until $|\omega_{i,j}^{n+1} - \omega_{i,j}^{n}| < 10^{-7}$ for steady flows. Details of the derivation of the formulation and
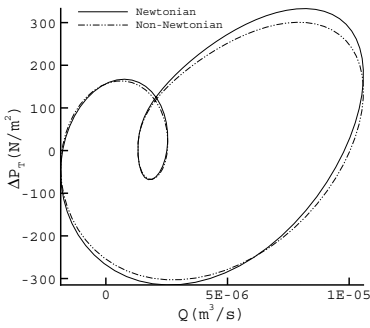
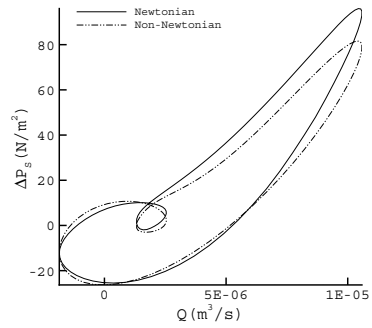Figure 5: $\Delta P_T - Q$ loop for physiological flow.

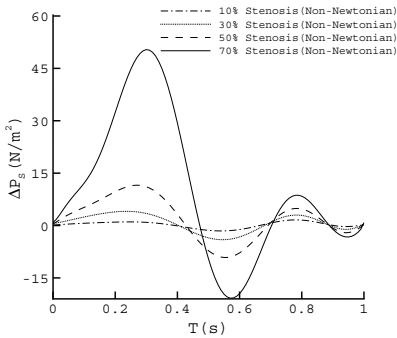Figure 6: $\Delta P_S - Q$ loop for physiological flow.

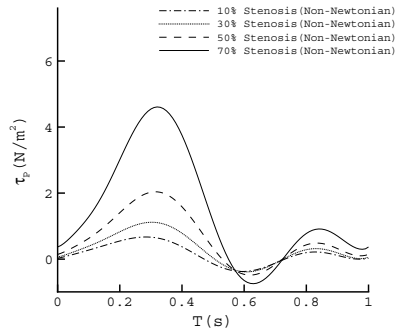Figure 7: Sensitivity of ΔP_S to varying degree of stenosis.

Figure 8: Sensitivity of τ_P to varying degree of stenosis.

numerical implementation will be presented in an upcoming journal paper. It should be noted that the current fluid model has been systematically validated with experimental and analytical results for steady and unsteady flows with and without stenosis. Systematic convergence studies have also been conducted. However, due to space limitations, validation studies will not be shown in this paper.

2.2 Comparison of hemodynamic parameters

To simulate physiological flow, the flow rate (Q) waveform shown in the dashed line in Fig. 2 is applied. The period is $1s$ and the Womersley number is 1.25. The peak Reynolds number ($Re \equiv \rho U_0 R / \mu_0$) is 132.5. Due to inertial and viscous

effects of pulsatile flow, there is a phase lag between the flow rate and other flow quantities. The phase shift between the total pressure drop ΔP_T (difference in P between the upstream and downstream boundaries) and the flow rate Q is shown in Fig. 2, which can also be presented in the form of a Lissajous figure in Fig. 5. The area inside the ΔP_T-Q loop corresponds to the rate of the viscous energy dissipation (ΔE_T). The width and slope of ΔP_T-Q loop correspond to the phase shift and resistance, respectively. The predicted instantaneous streamlines for both Newtonian and non-Newtonian flows are shown in Figs. 3 and 4, respectively, for every tenth of a cycle. The results compare well with FEM predictions shown in Ref. [15, Fig.8].

The total pressure drop, ΔP_T, is not very sensitive to the degree of stenosis because the effect of the stenosis is lumped together with inertial and viscous effects of pulsatile flow over a long, straight vessel. To isolate the influence of the stenosis, the pressure drop over a straight vessel (which can be obtained from Womersley's solution [16]) is subtracted from the total pressure drop, which gives the pressure drop due solely to the stenosis (ΔP_S). Comparison of the ΔP_S-Q loop between Newtonian and non-Newtonian flows is shown in Fig. 6, the area inside the loops corresponds to the rate of the viscous energy dissipation due solely to the stenosis (ΔE_S). The results indicate that the non-Newtonian behavior caused a slight decrease in pressure drop and modified the slope of the ΔP_S-Q curve, but has negligible influence on the rate of viscous energy dissipation.

The sensitivity of four parameters (the peak pressure drop due to the stenosis ΔP_S, the peak wall shear stress τ_P, the peak velocity U_P, and the rate of energy dissipation due to the stenosis ΔE_S) to varying degrees of stenosis is shown in Figs. 7 to 10. The results in all four figures are obtained using the non-Newtonian model. The degree of stenosis (α) is defined as $\Delta A/A_0 \times 100\%$, where ΔA is the area reduction due to stenosis and A_0 is the original lumen area without the stenosis. The comparison of the various hemodynamic parameters for varying degree of stenosis is shown in Figs. 11. The parameters are non-dimensionalized as follows:

$$\Delta = \frac{\xi - \xi_0}{\xi_{70} - \xi_0} \tag{13}$$

where ξ refers to the four candidate parameters (ΔP_S, τ_P, U_P, and ΔE_S), ξ_0 corresponds to the case without stenosis, and ξ_{70} corresponds to the case with 70% stenosis.

It can be observed that the rate of viscous energy dissipation due to the stenosis, ΔE_S, is the most sensitive to the increasing of degree of stenosis. Thus, in order to reliably detect stenosis at the earliest stage, ΔE_S should be used as the hemodynamic indicator, which can be related to degree of stenosis by fitting a cubic polynomial to the numerical or experimental data:

$$\Delta E_S = \sum_{i=0}^{i=3} c_i \alpha^i \tag{14}$$

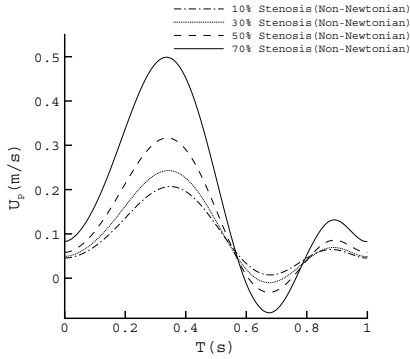where c_i is the ith coefficient of the cubic polynomial.

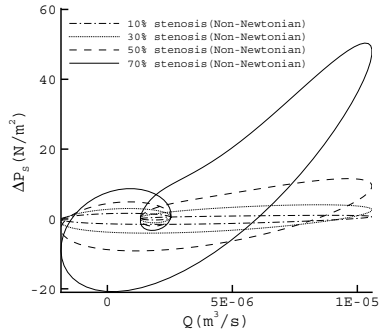Figure 9: Sensitivity of U_P to varying degree of stenosis.

Figure 10: Sensitivity of ΔE_S to varying degree of stenosis.
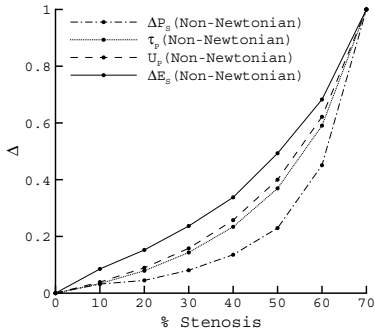

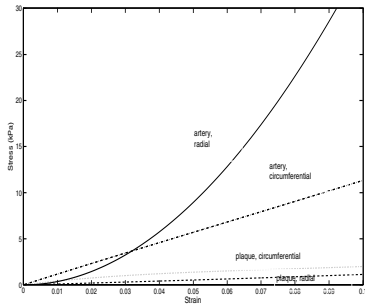Figure 11: Correlation between degree of stenoses and different hemodynamic parameters.

Figure 12: Stress–strain relations for the arterial wall and atheromous plaque.

Given two pressure measurements (P_1 and P_2 from the two ends of the vessel) and one flow rate (Q) measurement, the ΔP_S-Q loop can be plotted, which allows the calculation of ΔE_S (the area inside the ΔP_S-Q loop). Hence, the degree of stenosis, α, can be determined by evaluating the root of Eqn. (14). In other words, this equation can be used to interpret the percentage stenosis based on *in situ* sensor readings. Wireless MEMS sensors can be implanted on the interior surface at the two ends of the vessel to measure P_1 and P_2, and a wireless magneto-hydrodynamic flow sensor can be used to measure Q *in situ*. A schematic diagram showing proposed placement of the sensors is shown in Fig. 1.

3 Material model

The MEMS pressure sensor should be implanted on the interior surface of the vessel to provide maximum sensitivity to changes in pressure due to stenosis formation. It is possible that the sensor may itself become covered with an atheromic plaque. The utility of an implanted pressure sensor will depend upon the ability to diagnose accurately the formation of atherosclerotic plaques on the sensors themselves. Hence, a simplified material model is developed to investigate the sensitivity of the pressure measurements when obstructed by plaque formation.

The atherosclerotic artery is idealized as a set of nested cylinders with a pressure sensor placed at the interface between the arterial wall and the plaque. The cross-section of the artery is assumed to be axisymmetric, and the axial stress, σ_{xx}, is assumed to be zero. The viscous properties of the plaque and artery are ignored, and the stress through the plaque and artery is assumed to be zero when the internal pressure is zero. The axisymmetric equilibrium equation in polar coordinates is:

$$\sigma_{\theta\theta} = \sigma_{rr} + r\frac{\partial \sigma_{rr}}{\partial r}. \tag{15}$$

where $\sigma_{rr} = \sigma_{rr}(\epsilon_{rr})$ and $\sigma_{\theta\theta} = \sigma_{\theta\theta}(\epsilon_{\theta\theta})$ are the radial and circumferential stresses, respectively. The stresses vary with the radial position r, and are nonlinear functions of the radial ($\epsilon_{rr} = \frac{\partial u_r}{\partial r}$) and circumferential ($\epsilon_{\theta\theta} = \frac{u_r}{r}$) strains.

The strain-dependent tangential Young's moduli in the radial and circumferential directions are extracted from stress-strain relations for the plaque and artery wall. The importance of the mechanical properties of arterial tissue has long been recognized and has been measured since the latter part of the nineteenth century [17]. However, as summarized in the reviews presented in [18, 5], there is a general lack of reliable and consistent material data for both the arterial wall and plaque. In this work, the radial and circumferential properties of the plaque are obtained from Refs. [19] and [20], respectively; and the radial and circumferential properties of the arterial wall are obtained from Refs. [21] and [20], respectively. The resulting four stress-strain curves are shown in Fig. 12. Both tensile and compressive stresses and strains are shown as positive to fit all the data into one quadrant. It should be emphasized that the current material constitutive model is preliminary due to limited data, and should be updated when additional accurate and consistent measurements of the biaxial constitutive properties of the arterial wall and atherosclerotic plaque are available.

To show the effect of a plaque progressively covering an *in vivo* pressure sensor, the variation in stress through the thickness of the plaque and artery, and at the surface of the artery for varying thicknesses of plaque growth, is shown in Fig. 13. The data corresponds to a constant internal arterial pressure of 16 kPa for a 1mm thick artery of 2 mm internal radius. The value of the pressure reading for a sensor located at the interface between the plaque and arterial wall, again for a constant internal pressure of 16 kPa, is given in the inset in Fig. 13. The reduction in pressure at the sensor is a slightly non-linear function of the thickness of the overlying plaque for this range of plaque thicknesses.
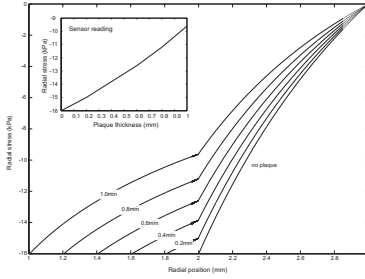
Figure 13: Radial stress for various plaque thicknesses on a 1mm thick artery with 2mm internal radius. Inlet: Radial stress at the interface between the plaque and the arterial wall.
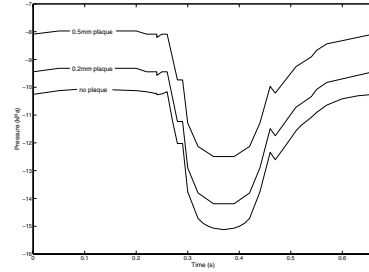
Figure 14: Time–pressure relation for an arterial graft near the aorta for increasing obstruction by atheromous plaque.

Figure 14 shows the time versus pressure curve for an unobstructed aorta over one heartbeat; these data are taken from [22]. A bypass graft typically leads to the heart from the aorta or a blood vessel near the aorta, and hence the aortic pressure can be taken as a good approximation to the actual pressure in the bypass graft. The time versus pressure relations of pressure readings by sensors obstructed by atheromous plaque of different thicknesses are given in the same figure. Clearly the pressure sensor provides intelligible data despite obstruction by growing plaque.

4 Sensor design

The actual sensing of the local pressure in the blood vessel can be done using MEMS pressure sensors [23, 24], similar to those shown in Figure 15. A wide range of such sensors has been developed for blood pressure measurements [23, 24, 25]. However, these are typically fabricated from silicon, which is not the most biocompatible material for long-term use in the human body. This section discusses diaphragm sensors that could be used to measure blood pressure *in-situ*, and explores the potential use of titanium and glycocalyx-like layers in the coating of silicon for improved biocompatibility and resistance to platelet adhesion.

4.1 Pressure sensing

Implantable diaphragm sensors were first proposed about two decades ago [24], and have been used recently in the *in situ* monitoring of blood pressure in animals [25]. An example of a blood pressure sensor is presented in Fig. 15. This consists of
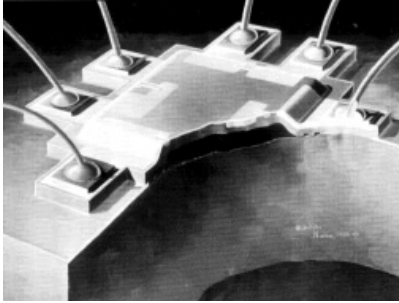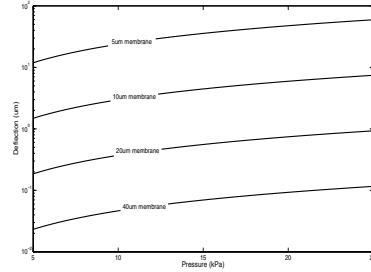
Figure 15: A MEMS pressure sensor.

Figure 16: Membrane deflection for various membrane thicknesses on a 1 mm diameter MEMS sensor.

silicon MEMS substrate with a thin layer of piezoelectric material. The membrane deflects due to the application of pressure, and the deflection gives rise to a wireless receiver at a local or remote site [25]. Hence, the possible onset of stenosis and restenosis can be detected using an implantable pressure sensor.

The mechanics of sensing relies strongly on membrane mechanics. For a circular diaphragm mounted on an O-ring, the maximum deflection, δ, of the membrane is given by [26]:

$$\delta = \frac{Pa^4(5 + \nu)}{64D(1 + \nu)} \tag{16}$$

where P is the pressure on the membrane, ν is the Poissons ratio, and a is the radius of the membrane. The variable $D = Et^3/12(1 - \nu^2)$ is given by the membrane thickness (t), Young's modulus of the silicon layer (E), and ν. For silicon MEMS, typical values of E are between 150 GPa and 220 GPa [27, 28]. An average Young's modulus of 175 GPa can be used for design estimates. Typical film thickness are in the range between 1 μm and 20 μm [23, 24]. Thus, Eqn. (16) can be use to develop design criteria for MEMS pressure sensing. Predictions of diaphragm deflection are presented in Fig. 16 for a range of clinically relevant pressures. For a 1mm diameter pressure sensor, detectable deflections exist for normal biological pressures if the membrane is less than 20 μm thick.

4.2 MEMS reliability

The maximum moment, M_{max}, and the maximum bending stress, σ_{max}, are given by:

$$M_{max} = \frac{Pa^2(3t\nu)}{16} \qquad \sigma_{max} = \frac{6M_{max}}{t^2} \tag{17}$$

Silicon has been shown to exhibit susceptibility to failure [29, 30, 31]. Thus, the objective should be to fabricate structures with stresses below the endurance limit, σ_e. Since there is no existing data for polysilicon MEMS in biomedical environments, a further reduction factor, β, must be applied to the design of reliable silicon pressure sensors:

$$\sigma_{max} < \frac{\sigma_e}{\beta} \tag{18}$$

where β should be a number greater than 1. Thus, the optimum design condition is the thickness that optimizes the deflection and the stresses in the membrane within the constraints implied by Eqns. (16) and (18).

4.3 Biocompatibility and adhesion/non-adhesion

One of the major obstacles to the use of long-term silicon in the body is the issue of biocompatibility and adhesion/non-adhesion [28, 32, 33]. Silicon is one of the materials that can elicit cytotoxic response in the body. Hence, there is the need to consider the coating of silicon with biocompatible materials. One possible approach is to use nano-scale titanium coatings (which have been shown to elicit no cytotoxic responses in the human body) to improve the biocompatibility of silicon surfaces. A recent paper by [33] suggested that nano-scale Ti coatings with thicknesses of approximately 50 nm are sufficient to promote cell spreading and adhesion that is comparable to that observed on titanium surfaces. However, the long-term stability and corrosion behavior of these layers is yet to be studied in biological environments that simulate the behavior of body fluids. Nevertheless, the pasivating nature of surface oxide films on silicon and titanium surfaces suggests that the films should be durable in the chemically aggressive environment in the human body. Another approach is to use polymeric layers, such as a glycocalyx-like coating, on silicon. Glycocalyx is known to reduce the adhesion of blood platelets to blood vessels, and have the advantages of being biocompatible. However, the long-term stability of glycocalyx-like and polymeric coatings is unclear. Thus, there may be a need to engineer self-healing polymeric layers that can replenish themselves over time, which is a challenge for future work. A third approach is a combination of the first and the second approaches. The titanium coatings provide biocompatibility and corrosion resistance, while the upper polymeric or glycocalyx-like layers provide non-stick surfaces that do not adhere to blood platelets. These can be conjugated directly to amine groups that are attached to titanium surfaces using chemistry described in [33].

5 Implications/conclusions

This paper presents analysis and ideas required for the design of implantable MEMS sensors for the *in situ* monitoring of blood flow. A CFD model has been developed for the simulation of unsteady, non-Newtonian flow around stenotic vessels. A plaque and arterial wall material model has been constructed to examine the sensitivity of pressure measurements to progressive plaque formation. Possible

design configurations and surface coating options have been presented for long-term monitoring of blood flow *in-situ*. A summary of the findings is presented below:

- Compared to other hemodynamic parameters, the rate of energy dissipation due to stenosis correlated best with increasing degree of stenosis.
- The interior pressure sensors should be able to provide intelligible data regarding occlusion risk despite possible obstruction by growing plaque.
- Diaphragm silicon pressure sensors with piezoelectric surface layers provide a robust platform for the design of implantable bioMEMS sensors, and the biocompatibility and non-adhesion properties of silicon sensors can be improved by the use of nanoscale metallic titanium layers and polymeric layers such as glycocalyx.

It should be noted that while these models are simplifications of the actual complex behaviour of the blood flow, the visco-elastic behaviour of the stenosed artery, and the operation of the sensors, they demonstrate that MEMS pressure sensors are legitimate candidates for use as *in vivo* blood pressure monitors. To develop a complete system for early stenosis detection, a magnetohydrodynamic (MHD) flow meter is also being investigated. The MHD meter will consist of a pair of magnets and a set of electrodes oriented orthogonally around the exterior of the blood vessel. Voltage signals due to MHD displacement current can be detected and interpreted to determine flow rates in the graft. Coupled with a wireless transmitter, these sensors offer the possibility of long-term *in vivo* monitoring of bypass graft or stent performance.

References

[1] TexasHeartInstitute. *http://www.texasheartinstitute.org/cad.html*, 2004.

[2] TexasHeartInstitute. *http://www.tmc.edu/thi/cab.html*, 2004.

[3] Yucel, E.K., Anderson, C.M., Edelman, R.R., Grist, T.M., Baum, R.A., Manning, W.J., Culebras, A. & Pearce, W., Magnetic resonance angiography update on applications for extracranial arteries. *Circulation*, **100**, pp. 2284–2301, 1999.

[4] Langerak, S.E., Vliegen, H.W., Jukema, J.W., Kunz, P., Zwinderman, A.H., Lamb, H.J., Wall, E.E. & Roos, A., Values of magnetic resonance imaging for the noninvasive detection of stenosis in coronary artery bypass grafts and recipient coronary arteries. *Circulation*, **107**, pp. 1502–1507, 2003.

[5] Steeves, C.A., Young, Y.L., Liu, Z., Babat, A., Bhalerao, K., Soboyejo, A.B.O. & Soboyejo, W.O., Design of implantable MEMS sensors for the in situ monitoring of blood flow. *submitted to the Journal of Materials Science: Materials in Medicine*, 2004.

[6] Liu, Z. & Young, Y., Comparison of hemodynamic parameteres for stenosis assessment. *Journal of Biomecanics*, **submitted**, 2005.

[7] Blechman, S., Z. O. amd Einav & Eldar, M., Method for determining the degree of occlusion and elasticity in blood vessels and other conducts. *U S Patent*, **6,129,674**, 2000.

[8] Blechman, Z.O., Einav, S., Zaretsky, U., Castel, D., Toledo, E. & Eldar, M., The area of the pressure-flow loop for assessment of arterial stenosis: A new index. *Technology and Health Care*, **10**, pp. 39–56, 2002.

[9] Wootton, D. & Ku, D., Fluid mechanics of vascular systems, diseases, and thrombosis. *Annual Reviews of Biomedical Engineering*, **1**, pp. 299–329, 1999.

[10] Berger, S. & Jou, L., Flows in stenotic vessels. *Annual Reviews of Fluid Mechanics*, **32**, pp. 347–382, 2000.

[11] Young, D. & Tsai, F., Flow characteristics in models of arterial stenosis - i. steady flow. *Journal of Biomechanics*, **6**, pp. pp. 395–410, 1973.

[12] Crochet, M.J., Debbaut, B., Keunings, R. & Marchal, J.M., Polyflow: a multi-purpose finite-element program for continuous polymer flows. *Computer Modeling of Extrusion and Other Continuous Processes*, Hanser, Munich, pp. 25–50, 1992.

[13] Williamson, J.H., Low-storage *runge-kutta* schemes. *Journal of Computational Physics*, **35**, pp. 48–56, 1980.

[14] Chung, T.J., *Computational Fluid Dynamics*. Cambridge University Press: New York, 2002.

[15] Tu, C., Deville, M. & Vanderschuren, L., Finite element simulation of pulsatile flow through arterial stenosis. *Journal of Biomechanics*, **25**, pp. pp.1141–1152, (1992).

[16] Womersley, J.R., Method for the calculation of velocity, rate of flow and viscous drag in arteries when the pressure gradient is known. *Journal of Physiology*, **127**, pp. 553–563, 1955.

[17] Roy, C.S., The elastic properties of the arterial wall. *Journal of Physiology*, **3**, pp. 125–162, 1880.

[18] Salunke, N.V. & Topoleski, L.D.T., Biomechanics of atherosclerotic plaque. *Critical Reviews in Biomechanical Engineering*, **25(3)**, pp. 243–285, 1997.

[19] Lee, R.T., Richardson, S.G., Loree, H.M., Grodzinsky, A.J., Gharib, S.A., Schoen, F.J. & Pandian, N., Prediction of mechanical properties of human atherosclerotic tissue bu high-frequency intravascular ultrasound imaging. *Arteriosclerosis and Thrombosis*, **12**, pp. 1–5, 1992.

[20] Hayashi, K. & Imai, Y., Tensile property of atheromatous plaque and an analysis of stress in atherosclerotic wall. *Journal of Biomechanics*, **30(6)**, pp. 573–579, 1997.

[21] Patel, D.J., Janicki, J.S. & Carew, T.E., Static anistropic elastic properties of the aorta in living dogs. *Circulation Research*, **25**, pp. 765–779, 1969.

[22] Fung, Y.C., *Biodynamics: Circulation*. Springer-Verlag: New York, 1984.

[23] Kovacs, G.T.A., *Micromachined Transducers Handbook*. McGraw Hill: New York, 1998.

[24] Madou, M., *Fundamentals of Microfabrication*. CRC Press: Boca Raton, FL, 2nd edition, 2002.

[25] Bhalerao, K., Mwenifumbo, S., Soboyejo, A.B.O. & Soboyejo, W.O., Bounds in the sensitivity of bioMEMS devices for cell detection. *Nanotechnology*, **6**, pp. 23–31, 2004.

[26] Timoshenko, S., *Theory of Plates and Shells*. McGraw Hill: New York, 1959.

[27] Sharpe, W.N., Brown, S., Johnson, G.C. & Knauss, W., Round-robin tests of modulus and strength of polysilicon. *Proc. Microelectromechanical Structures for Materials Research*, San Francisco, CA, pp. 57–65, 1998.

[28] Ratner, B.D., Hoffman, A.S., Schoen, F.J. & Lemmons, J.E., *Biomaterials Science: An Introduction to Materials Science in Medicine*. Academic Press: San Diego, CA, 2nd edition, 2004.

[29] Arsdell, W.V. & Brown, S., Sub-critical crack growth in silicon MEMS. *Journal of Microelectromechanical Systems*, **8**, pp. 319–327, 1999.

[30] Allameh, S.A., Shrotriya, P., Butterwick, A., Brown, S.B. & Soboyejo, W.O., Surface topography evolution and fatigue fracture in polysilicon MEMS structures. *Journal of Microelectromechanical Systems*, **12**, pp. 313–324, 2003.

[31] Shrotriya, P., Allameh, S., Brown, S.B., Suo, Z. & Soboyejo, W.O., Fatigue damage evolution in silicon films for micromechanical applications. *Experimental Mechanics*, **43**, pp. 289–302, 2003.

[32] Brunette, D.M., Tengvall, P., Textor, M. & Thompsen, P., *Titanium in Medicine: Materials Science, Surface Science, Engineering, Biological Responses and Medical Applications*. Springer: New York, 2001.

[33] Milburn, C., Kung, E., Oparinde, G.M., Chen, J., Beye, A.C., Schwartz, J. & Soboyejo, W.O., Effects of RGD and nanoscale titanium coatings on cell spreading and adhesion. submitted to *Journal of Materials Science: Materials in Medicine*, 2004.